P H Y S I C A L   R E V I E W   L E T T E R S

Atomistic Simulation of the Transition from Atomistic to Macroscopic Cratering

Juha Samela[*] and Kai Nordlund

Department of Physics, P.O. Box 43, FI-00014, University of Helsinki, Finland

Using large-scale atomistic simulations, we show that the macroscopic cratering behavior emerges for projectile impacts on Au at projectile sizes between 1000 and 10 000 Au atoms at impact velocities comparable to typical meteoroid velocities. In this size regime, we detect a compression of material in Au nanoparticle impacts similar to that observed for hypervelocity macroscopic impacts. The simulated crater volumes agree with the values calculated using the macroscopic crater size scaling law, in spite of a downwards extrapolation over more than 15 orders of magnitude in terms of the impactor volume. The result demonstrates that atomistic simulations can be used as a tool to understand the strength properties of materials in cases where only continuum models have been possible before.

Craters produced by meteorites, bullets, and other macroscopic objects are visible to the bare eye. However, a single atom can produce an atomic-scale nanocrater when it hits a dense material [1–3]. Although these craters do superficially resemble each other, their formation processes are different. The atomic-scale craters are formed by atomic displacement or flow processes that occur near the surface [3–5], while macroscopic crater formation is better understood in terms of a transient high-pressure region inside the material [6]. What has remained unclear is where the transition from the atomistic to the macroscopic cratering regime occurs. The understanding of how the effects of hypervelocity impacts emerge from atomic interactions is important for the construction of shielding materials for applications, where the materials are subject to small particle bombardment.

In this Letter we show with classical molecular dynamics that the macroscopic cratering behavior emerges from the basic interactions between the Au atoms in Au(111) at projectile sizes between 1000–10 000 Au atoms. This result forms a bridge between the microscopic and macroscopic lines of impact research by showing that the behavior of materials under macroscopic impacts can be understood and simulated from atomistic interactions, and shows that the macroscopic scaling applies even at projectile diameter less than 20 nm, although the scaling laws are originally developed for much larger impactors, such as meteoroids. The detection of the macroscopic scaling at the nanosize is interesting from the point of view of basic research. However, the result is also important in practice, because it demonstrates the possibility of studying the macroscopic effects of impacts starting from the atomistic interactions using small systems as prototypes.

Research of microscopic and macroscopic impacts have traditionally been rather separate fields of physics. The formation of craters by impacts of single atoms or small nanoclusters is reasonably well understood [7,8]. Cluster ion beams and scanning probe microscopy are important experimental methods, and effects of impacts are studied with molecular dynamics. In modern technology, beams of clusters of a few thousand atoms are routinely used for surface processing, chemical analysis, implantation, and creation of nanostructures [9–13]. On the other hand, in astronomy the impacts of asteroids with sizes up to tens of kilometers on moons and planets are studied because they provide information about the development of the solar system and have affected the evolution of life on Earth [14]. Good understanding of the formation of macroscopic craters induced by hypervelocity projectiles has been achieved by a combination of experimental observations of planetary craters [14], gas gun experiments [15], and modeling with hydrodynamic codes [16]. Micrometeorite and space debris impacts on spacecrafts are investigated to control their harmful effects [15,17]. In forensic science an important research theme is the effects of bullets on objects they hit [18].

To find the transition point from small cluster impact behavior to the macroscopic behavior, we have simulated impacts of large Au_N ($N = 13$–315 000) clusters on the Au(111) surface. The Au-Au interaction model used in our molecular dynamics simulations can describe well both high-energy atomic collisions and the thermodynamic behavior of the material [7,19], making it possible to use these models to search for the transition to the macroscopic regime. The velocity of the projectiles was chosen to be around 22 km/s to match that typical of meteoroid impacts. A uniform velocity perpendicular to the surface was given to all cluster atoms in the beginning of each simulation. The borders of the system were cooled to ambient temperature (150 K), and the volume of the simulation cell was kept constant. The effect of the boundary conditions on the simulation results is discussed in Ref. [20]. Electronic stopping of fast atoms was also part of the simulation model [19]. The simulated Au(111) substrate size was $100 \times 100 \times 100$ nm (61×10^6 atoms) or $200 \times 200 \times 60$ nm (144×10^6 atoms) depending on the impactor size. The depth of 60 nm is large enough for the crater induced by 500 eV/atom impacts, but the crown induced by a Au_{315000} cluster requires a wider area than $100 \times 100 \times 100$ nm to be completely simulated. Despite

the large size of the simulation box, the fingers of the largest corona reach the boundaries in the final stages of the corona development, but this does not affect the main conclusions of this study. Depending on the total cluster energy, total CPU times were 10 000–50 000 hours/impact, which limited our study to one or two simulations per cluster size and energy. However, the variation of crater volume is relatively small at large cluster sizes. The simulations were followed up to 50–250 ps depending on the impact energy. The Au-Au interaction potential used in this study is based on the corrected effective medium theory [21,22]. It gives sputtering yields that are in agreement with experimental results for Xe impacts on Au(111) [20] and for Au_{13} impacts on Au(111) [7]. Other details of the simulation method can be found in Refs. [7,19].

According to the simulations, the coherent interaction of atoms gradually leads to macroscopic impact behavior, when the size of the cluster increases. We observe that during the first phase of the impact, which lasts from 0.3– 1.0 ps, depending on the cluster energy and size, the cluster penetrates inside the substrate and only a small number of atoms are ejected from the substrate. In other words, the cluster atoms together with those substrate atoms that were initially located in the impact region are compressed inside the substrate (Fig. 1). The compressed region is formed because the number of atoms in the frontier increases while the cluster penetrates deeper in to the substrate, and the substrate arrests the expansion of the frontier. Also the projectile is gradually compressed in the high-pressure area (Fig. 2). Finally, the compressed region is almost an ellipsoid in the bottom of the cavity. In the second phase, this very dense, high-pressure region releases its energy radially forming a hemispherical cavity of hot material which escapes to the vacuum leaving a crater.

A similar two-phase compression or radial expansion process is known to occur in macroscopic hypervelocity impacts [6]. Compression of projectile and target materials, the isobaric core, occurs in the first phase of planetary impact events [23,24]. The biggest terrestrial craters are caused by impactors of similar size and velocity. In these simulations [16,23], the transient forms of the cavity and corona are very similar to the forms shown in our simulations of atomic cluster impacts. By contrast, no clear compressed region is observed in the atom or small cluster impact simulations even at considerable higher energies than 500 eV/atom [7]. (See also the supplementary EPAPS document [25]). Thus, we conclude that the appearance of this region in the large cluster impact simulations is a clear indication of the shift towards macroscopic behavior.

The crater volume scales linearly with the impactor size only when most of the impact energy is first stored in the compressed region and after that released radially so that it destroys the structure in a hemispherical volume. The volume depends linearly on the energy and hence also on N. If a considerable amount of impact energy is released to the vacuum already during the cavity expansion phase, as happens in the small cluster impacts, the crater volume scaling is not linear. The neighborhood density distribution in Fig. 2 shows quantitatively that clear compressed region appears gradually between $N = 1000$–6000. Thus, some compression can be detected at smaller N than the linear scaling regime, but the compression/radial expansion mechanism becomes dominant only gradually. The highest density found in this study is almost 4 times the normal density of solid Au (for 5 keV/atom Au_{168000}).
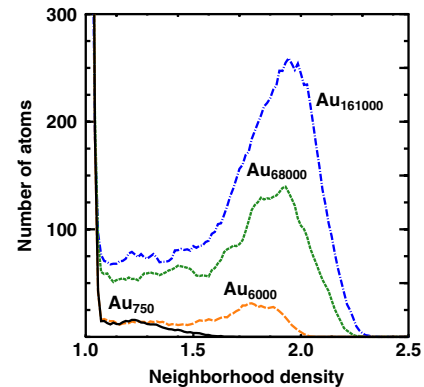
FIG. 2 (color online). The distribution of number densities in the impact region at the moment when the highest density occurs at different cluster sizes from 750 to 161 000 atoms. The ordinate indicates how many atoms in the volume surrounding the compressed region and cavity have a given number density around it. The histogram bin in the ordinate is 1 atom/nm³. The relative number density around an atom is calculated by counting the number of neighbor atoms in the 1 nm³ neighborhood of the atom and dividing this by 69 atoms/nm³ (number density of bulk Au). The densities are calculated for atoms in a region which is of the same size in all cases (17.0 × 0.5 × 24.0 nm slice around the cavity).
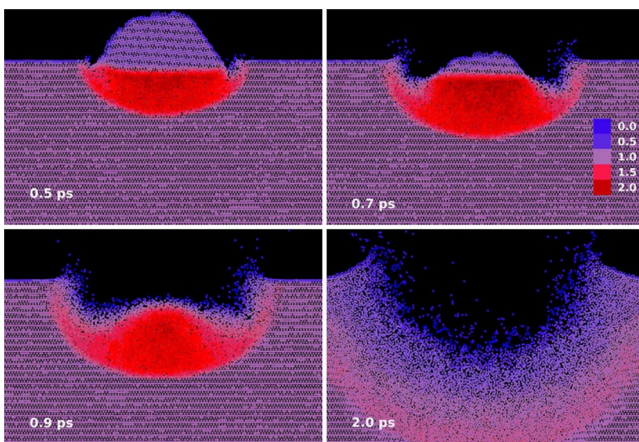
FIG. 1 (color online). Visualization of the compression of material in the stopping phase. The neighborhood density of atoms in impact region at 500–2000 fs after an impact of an Au_{68000} atomic cluster with energy 500 eV/atom. (Neighborhood density is defined in the caption of Fig. 2). The high density core region is shown in dark gray. The panel size is 3.4 × 2.3 nm.

Figure 3 shows how the pressure is released during the first 3 ps after the impact. At 1 ps, both the untouched substrate material (69 atom/nm^3) and the compressed material are present. At 2 ps, most of the compression has released and a low-density region is shown in the distribution, indicating that the substrate is partly in the gaseous state. At 3 ps, the crystal structure is almost completely destroyed in the volume considered.

In the macroscopic strength regime, the crater volumes V have empirically been found to follow the behavior

$$V = K_1 \frac{m}{\rho} \left(\frac{\rho U^2}{\bar{Y}} \right)^{3\mu/2}, \tag{1}$$

where U is the impactor velocity, m is the impactor mass, and ρ is the density of the material. $\bar{Y}$, μ, and K_1 are parameters that depend on the strength of the material [26]. Figure 4 shows that the simulated volumes indeed converge towards the estimated macroscopic value $V/N =$ 0.17 nm^3. The value is gained from Eq. (1) using empirical parameters $K_1 = 0.2$ and $\mu = 0.55$ for hard rock [26], Young's modulus $Y = 78$ GPa, and density $\rho =$ 19 300 kg/m^3 for Au. (See the EPAPS document [25] for more details.) From this result, we cannot definitely conclude that the simulations and the empirical scaling law agree quantitatively because empirical scaling parameters are not available for Au [25]. However, we can say that with a reasonable choice of parameters, like the parameter set mentioned above, one gets an estimate of crater volume which is of about the same magnitude as the simulated volume. This result is not evident because the macroscopic scaling is derived for impactors that are more than 15 orders of magnitude larger in number of atoms than the clusters in this study; thus, the empirical law is extrapolated downwards by more than 15 orders of magnitude. Most important, however, is the observation that the simu-
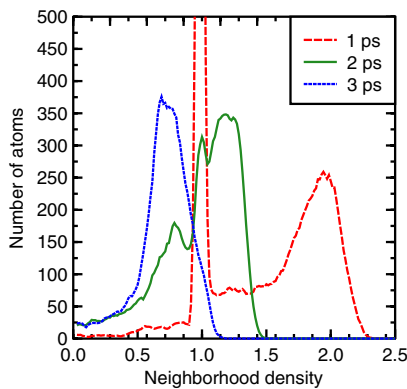
lated scaling of crater volumes becomes linear with projectile size (Fig. 4), which is typical for the macroscopic impacts [26]. In small cluster impacts, the volume increases nonlinearly with N (Fig. 4 and [8]).

However, the crater volume per cluster atom is smaller in the macroscopic regime than it is in the case of small clusters (Fig. 4). This is related to the fact that a relatively large proportion of the impact energy is dissipated outside the displacement cascade by the shock wave and thermal conduction in the macroscopic impacts. In small cluster impacts, energy is considerably moved from the cavity by immediate sputtering.

From Eq. (1), the ratio between crater volumes of impacts with velocities U_1 and U_2 is $V_1/V_2 = (U_1/U_2)^{3\mu}$. When $U_1 = 70$ km/s, $U_2 = 20$ km/s, and $\mu = 0.55$ [26], the ratio is 7.9. From simulations we detected corresponding ratios 7.2 at $N = 750$ and 8.3 at $N = 6000$. This indicates that the crater volumes in the atomistic simulations scale also with the velocity according to the macroscopic scaling law [Eq. (1)] already at relatively small impactor sizes. Thus, the macroscopic scaling with velocity begins at lower impactor sizes than the macroscopic scaling with impactor size. When the impact energy is higher than 25 keV/atom, the transition to macroscopic scaling probably occur at larger impactor sizes, because the channelling probability increases and therefore some cluster atoms loose their energy outside the compression region [25]. At lower energies than 5 keV/atom, the scaling behavior detected in the simulations is valid as long as the impactor has enough energy to penetrate inside the substrate. Then most of the energy of the compressed region is used to expand the crater, which leads to the linear scaling of crater volume with number of atoms in the impactor.

The shape of the transient crater rim follows the crystallographic directions of the Au(111) surface (Fig. 5). These patterns appearing around the crater region resemble those observed [27] and simulated [28] in nanoindentation studies. The strong pressure wave emanating from the cascade causes entire planes of atoms to slide coherently
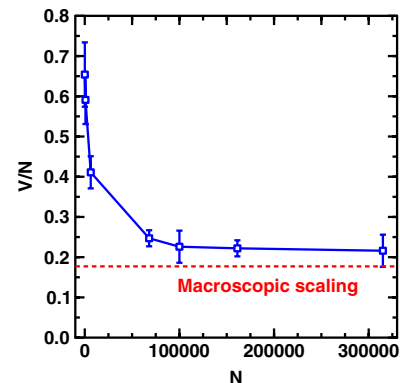
FIG. 3 (color online). Evolution of the neighborhood density distribution in the impact region in a 500 eV/atom Au$_{161000}$ impact. The peaks at 1 and 2 ps correspond to the compressed region in Fig. 1. The low-density peak at 3 ps describes the evaporation of high-energy atoms from the cavity walls (last frame of Fig. 1). Notice that the development is faster in the Au$_{68000}$ event (Fig. 1) than in the Au$_{161000}$ event (this figure). In general, the duration of cratering increases with projectile size.

FIG. 4 (color online). Crater volume per number of atoms in the impacting cluster (V/N) as a function of cluster size showing the transition from nonlinear scaling to linear scaling.
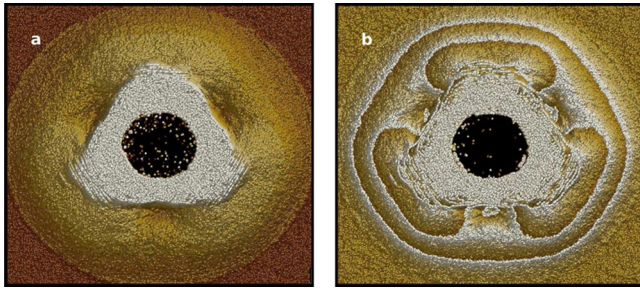
FIG. 5 (color online). Effect of crystal orientation. Transient patterns around the crater at 18 ps after an impact of 500 eV/atom Au_{315000} projectile. Both panels are 200×200 nm showing a 2 nm slice above the surface (a) and 1 nm slice just beneath the surface (b). The atoms are colored according to the distance from the viewer. See the EPAPS document for more examples [25].

along the {111} planes of fcc metals [29]. If defects are present in the substrate, the impact may induce cracks near the crater, and then fragments of material are ejected into the vacuum, increasing the sputtering yield. Although this is not observed in the simulations due to the perfect Au(111) structure, the ejection of fragments is another characteristic feature of macroscopic impact. The results demonstrate that the understanding of macroscopic impacts in the atomic level is now possible, which may benefit cracking research and design of materials.

After the energy released from the compressed region has melted the surrounding substrate, the ejection of atoms occurs in two phases. First, the high-energy atoms in the center of the cavity escape directly to vacuum. Second, the liquid phase atoms in the outer rim of the cavity form a corona around the cavity opening (Fig. 1). The corona releases material in clusters [19]. In the molecular dynamics simulations, the ejection of material lasts 100–300 ps until the corona cools down to the ambient temperature and forms the crater rim [19]. These two ejection phases are typical not only for large clusters, but they occur also with small clusters ($N = 5$–13), if their energy is several keV/atom [7]. However, swift ions and small clusters (100–1000 keV/atom) can channel deep into the substrate in crystalline materials, which leads to a decreased ejection yield [7]. At even higher energies, the electronic stopping dominates and cratering mechanisms are different. In addition to the compression phenomenon, another macroscopic feature seen in the simulations is the emergence of fingers in the corona around the cavity [25].

*juha.samela@helsinki.fi

[1] K. L. Merkle and W. Jger, Philos. Mag. A **44**, 741 (1981).
[2] F. Thibaudau, J. Cousty, E. Balanzat, and S. Bouffard, Phys. Rev. Lett. **67**, 1582 (1991).
[3] M. Ghaly and R. S. Averback, Phys. Rev. Lett. **72**, 364 (1994).
[4] R. Aderjan and H. M. Urbassek, Nucl. Instrum. Methods Phys. Res., Sect. B **164**, 697 (2000).
[5] K. Nordlund, K. O. E. Henriksson, and J. Keinonen, Appl. Phys. Lett. **79**, 3624 (2001).
[6] R. M. Schmidt and K. R. Housen, Int. J. Impact Eng. **5**, 543 (1987).
[7] J. Samela and K. Nordlund, Phys. Rev. B **76**, 125434 (2007).
[8] J. Samela and K. Nordlund (to be published).
[9] G. Hubler, Surf. Coat. Technol. **158**, 449 (2002).
[10] D. G. Castner, Nature (London) **422**, 129 (2003).
[11] A. Kirkpatrick, Nucl. Instrum. Methods Phys. Res., Sect. B **206**, 830 (2003).
[12] V. N. Popok and E. E. B. Campbell, Reviews on Advanced Materials Science **11**, 19 (2006).
[13] N. Winograd, Z. Postawa, J. Cheng, C. Szakal, J. Kozole, and B. J. Garrison, Appl. Surf. Sci. **252**, 6836 (2006).
[14] M. V. Gerasimov, B. A. Ivanov, O. I. Yakovlev, and Y. P. Dikov, Earth Moon Planets **80**, 209 (1998).
[15] V. Jantou, D. McPhail, R. Chater, and A. Kearsley, Appl. Surf. Sci. **252**, 7120 (2006).
[16] D. de Niem, E. Khrt, and U. Motschmann, Planet. Space Sci. **55**, 900 (2007).
[17] A. Kearsley, G. Graham, J. McDonnell, E. Taylor, G. Drolshagen, R. Chater, D. McPhail, and M. Burchell, Adv. Space Res. **39**, 590 (2007).
[18] M. Thalia, B. Kneubuehl, U. Zollinger, and R. Dirnhofer, Forensic science international **132**, 93 (2003).
[19] J. Samela and K. Nordlund, Nucl. Instrum. Methods Phys. Res., Sect. B **263**, 375 (2007).
[20] J. Samela, J. Kotakoski, K. Nordlund, and J. Keinonen, Nucl. Instrum. Methods Phys. Res., Sect. B **239**, 331 (2005).
[21] J. D. Kress and A. E. DePristo, J. Chem. Phys. **88**, 2596 (1988).
[22] C. L. Kelchner, D. M. Halstead, N. M. W. L. S. Perkins, and A. E. DePristo, Surf. Sci. **310**, 425 (1994).
[23] E. Pierazzo, A. M. Vickery, and H. J. Melosh, Icarus **127**, 408 (1997).
[24] H. J. Melosh and B. A. Ivanov, Annu. Rev. Earth Planet Sci. **27**, 385 (1999).
[25] See EPAPS Document No. E-PRLTAO-101-048829 for supplementary information and more examples. For more information on EPAPS, see http:// www.aip.org/pubservs/epaps.html.
[26] K. A. Holsapple, Annu. Rev. Earth Planet Sci. **21**, 333 (1993).
[27] Y. Wang, D. Raabe, C. Klber, and F. Roters, Acta Mater. **52**, 2229 (2004).
[28] H.-P. Chen, T. K. Kalia, A. Nakano, P. Vashishta, and I. Szlufarska, J. Appl. Phys. **102**, 063514 (2007).
[29] K. Nordlund, J. Keinonen, M. Ghaly, and R. S. Averback, Nature (London) **398**, 49 (1999).